Numerical Methods in Civil Engineering, 6-2 (2021) 36-48

Numerical Methods in Civil Engineering

Journal Homepage: https://nmce.kntu.ac.ir/

Investigation of Hydrodynamic Characteristics of Flow Caused by Dam Break around a Downstream Obstacle Considering Different Reservoir Shapes

Atabak Feizi*, Aysan Ezati, Shadi Alizadeh Marallo*****

ARTICLE INFO

RESEARCH PAPER

Article history:
Received:
June 2021.
Revised:
July 2021.
Accepted:
August 2021.

Keywords:
Dam break;
Reservoir geometric shape; Obstacle;
Flow hydrodynamics;
Numerical modeling

Abstract:

Dams are important structures that are mainly constructed for water and energy supply. Dam break creates a huge flow that leads to flooding in areas downstream. Therefore, determining characteristics of this flow, including the flow depth and wave propagation velocity, is of great importance. In this research, the simultaneous effects of reservoir geometries and downstream obstacles on hydrodynamic characteristics of the flow caused by dam break have been investigated using three-dimensional numerical modeling. For this purpose, six reservoirs with different geometries, including wide, trapezoidal, L-shaped, long, hexagonal, and octagonal reservoirs, with downstream dry beds have been considered. The results of three-dimensional numerical modeling indicate that the reservoir geometric shape has a severe effect on the flow, since it plays a determining role in the inlet flow to the downstream channel. Downstream obstacles also affect the flow caused by dam break, but their effects are local and significant only over a certain length behind obstacles. This length is related to the reservoir shape and varies within the range of 19.5 to 22.5 times the pier (obstacle) diameter. Thus, the largest length in which the local effects are significant is observed in the wide reservoir, which is approximately 22.5 times the pier diameter. Meanwhile, the minimum length is related to the long reservoir, which is 19.5 times the pier diameter.

1. Introduction

Dams are important structures that are constructed to collect and store water for electricity generation, irrigation and flood control. Despite all efforts to improve the safety of dams, sometimes due to insufficiency of the weir, earthquake, defect of the foundation, and other reasons, the dam could fail [1]. In the recent decade, much research aiming at dam break has been carried out; because the flow caused by dam break is an unsteady and nonlinear flow that can lead to serious damage to urban areas and agricultural lands lying downstream.

* *Corresponding author: Associate Professor, Dept. of Civil Engineering, Faculty of Engineering, University of Mohaghegh Ardabili, Ardabil, Iran. E-mail: a_feizi@uma.ac.ir*
** *M.Sc. Student of Civil Engineering — Water Resources Management and Engineering, Dept. of Civil Engineering, University of Mohaghegh Ardabili, Ardabil, Iran.*
*** *M.Sc. Student of Civil Engineering — Water and Hydraulic Structures Engineering, Dept. of Civil Engineering, University of Mohaghegh Ardabili, Ardabil, Iran.*

One of the most critical issues in the dam break phenomenon is the study of flow patterns around downstream obstacles due to the flow caused by dam break. The accurate prediction of characteristics of waves created by dam break, including the wave propagation velocity, submergence depth, and flood timing, reduces damage resulting from dam break [2]. Soares-Frazão and Zech [3] investigated the dam break at a 90 ° bend, dry bed, and rectangular channel. In this study, cameras installed at the top of the channel were used to measure the flow velocity and surface area. Water was used from the cameras located on the side of the channel. Comparison of the measured laboratory values with the results of one-dimensional and two-dimensional numerical and hybrid models showed that the full two-dimensional model displays better results at 90 ° bend. The most important difference between the numerical results and laboratory values is due to the impact of the rejection wave to the bend. Soares-Frazão [4] investigated the wave propagation due to dam break and the effect of downstream barrier on the flow pattern in a tapered triangular channel with a dry bed experimentally. In this study, two

measurement tools were used to obtain the water level. The first was the use of resistance gauges with voltage changes, and the second was the use of high-speed digital cameras to measure the water level. In this study, the results of the two methods were compared at certain points. This comparison showed that the values obtained for the water level in both methods are very close to each other.

In another study, Soares-Frazão and Zech [5] examined the effect of downstream obstacles on the wave created by dam break experimentally. They used a rectangular channel containing a rectangular obstacle. The results showed that when the wave collides with the obstacle, the flow is diverted, and a hydraulic jump is formed. Then a wake zone is created behind the obstacle. Ozmen-Cagatay and Kocaman [6] investigated the flow caused by dam break in a channel with a dry bed and a trapezoidal obstacle located downstream, both experimentally and numerically. According to their results, as the flow collides with the obstacle, a reflective flow toward upstream is created. Thus, a combination of progressive and reflective flows is formed behind the obstacle. Also, they exploited a numerical model to obtain the flow field and water surface profile of the flooding across the dam.

Feizi et al. [7] studied the effect of reservoir geometric shapes on the flow caused by dam break in both dry and wet bed conditions. They considered four reservoirs with different geometries, including wide, trapezoidal, long and L-shaped reservoirs. Their study showed that long and L-shaped reservoirs lead to a similar trend due to forming a one-dimensional flow, and the results correspond to Ritter's analytical solution well. However, for wide and trapezoidal reservoirs, due to the formation of a two-dimensional flow pattern, the obtained results are not comparable with Ritter's analytical solution. Moreover, the wide reservoir leads to the highest water level and velocity, and meanwhile, a faster decline of these quantities compared to other geometries.

Aureli et al. [8] investigated the effect of downstream obstacles on the wave caused by dam break. They used three different models, including the 2-D depth-averaged model, 3-D Eulerian two-phase flow model, and Smoothed-particle Hydrodynamics (SPH). The results demonstrated that three-dimensional models simulate the dam break wave more precisely, in contrast, two-dimensional models based on SWE are not able to predict the hydrograph pick level for large waves accurately. However, the difference between the results of two-dimensional models and experimental data is about 10%; Therefore, two-dimensional models can also be used in practice. In terms of predicting flow fluctuations, the SPH model is the best option, and the other two models provide almost the same results for flow fluctuations.

Costabile et al. [9] investigated the wave propagation in rivers both in the presence and absence of a pier downstream. They used one-dimensional and two-dimensional numerical models based on SWE. In their study, due to the rectangular cross-section in most rivers, the one-dimensional model is proposed to predict the flow. By increasing the sensitivity of the project application, the two-dimensional model can replace the one-dimensional model.

Hooshyaripor and Tahershamsi [10] investigated the effect of the reservoir lateral slope on the dam break hydrograph and water free surface profile numerically and experimentally. They used an ideal trapezoidal reservoir with a variable lateral slope of 30˚ to 90˚. The results showed that as the lateral slope decreases, the peak flow rate increases, and the water surface curve reaches its maximum level faster. Consequently, the risks caused by dam break in a trapezoidal reservoir with a lower lateral slope (30˚) is higher. Javadian et al. [11] studied the dam break phenomenon experimentally. In their research, frontal wave velocity and volume of displaced water at different times are indicated. They are compared with theoretical results obtained from the characteristic method of analytical solution of Saint-Venant equations. The results indicate that the theoretical and experimental responses have a close agreement. The minor differences between the results originate from the assumptions implied in the Saint-Venant equations.

Jian et al. [12] studied dam break hydrodynamics in the presence of fixed and moving obstacles downstream. They utilized two different numerical methods, ISPH and WCSPH. Their study showed that the ISPH model performs better and obtains a larger number of pressure distribution and particle motion diagrams in a shorter time. Moradi Mofrad et al. [13] studied the turbulent flow caused by dam break around a trapezoidal obstacle downstream. According to their results, a portion of the flow passes through the obstacle, while the remaining flow, due to its insufficient energy, cannot pass through the obstacle and causes a reflective flow and a negative surge. Due to no flow passing through the obstacle, small surface waves are created that are able to pass through the obstacle as the specific energy of the flow increases. The flow pressure is initially hydrostatic and then decreases. At the point where the flow collides with the obstacle, the pressure increases and becomes dynamic.

Yilmaz et al. [14] investigated the flow caused by dam break in a channel with a triangular obstacle located downstream, using the finite element method. Their numerical results exhibit an acceptable coherence with the experimental data.

Amini et al. [15] investigated the Vahdat Dam break in Kurdistan Province of Iran and the resulting flood spread by combining the HEC-RAS and ArcMap software programs. The results showed that the type of dam break has a significant effect on the created hydraulic characteristics of the flow in the river downstream of the dam. If the dam break is gradual, choosing fission parameters estimation method will affect the characteristics of the wave break.

Azimi et al. [16] and Issakhov et al. [1] simulated the effect of different-shaped obstacles located downstream of a channel numerically using the Volume of Fluid (VOF)

method. Feizi [17] studied dam break flow hydrodynamics in the presence of a cylindrical obstacle downstream of a channel. He used two different reservoir geometries, wide and long. His results demonstrated that for the wide reservoir, a two-dimensional flow, and the long reservoir, a one-dimensional turbulent flow is formed. Saghi and Lakzian [18] investigated the effect of the geometric obstacle shape located downstream on the flow caused by dam break. According to their results, the triangular obstacle with a 55˚lateral slope is recommended as the obstacle with the optimum angle for mitigating the destructive effects of dam break. Issakhov and Imanberdiyeva [2] studied the dam break three-dimensional flow and water surface motion in the presence of a trapezoidal obstacle downstream. Wang et al. [19] investigated the dam break flow experimentally in both triangular and rectangular channels. Water surface profiles and stage hydrographs are obtained using video images. In their research, experimental measurements were performed in a straight and prismatic flume with a horizontal and wet bed. This study aimed to understand the effect of wet conditions downstream of dam break in triangular channels. Detailed experimental data are provided to validate both analytical and numerical solutions.

Monteiro et al. [20] investigated the effect of fluid pressure on multiphase flows with second-order accuracy in dam break problem numerically. This study provided the flow characteristics due to dam break in two modes of hydrostatic pressure and total pressure using the Navier-Stokes equations. The results showed that better results are obtained in the dam break problem by considering the total pressure instead of the hydrostatic pressure. Kocaman et al. [21] investigated the dam break flow in a channel with different lateral contractions downstream numerically and experimentally. They used a channel with three different lateral contractions; one triangular and two trapezoidal contractions with different slopes. According to their results, the lateral contraction causes a negative surge and eventually creates a hydraulic jump, while a portion of the flow goes downstream. Also, when the dam break flow passes through the contracted section downstream, a strong and unsteady reflective flow with a higher water level is observed upstream. The intensity of this reflective flow for the sharp trapezoidal obstacle is higher than that of the mild-sloped trapezoidal obstacle, and the least intensity is observed for the triangular obstacle.

Najar and Gul [22] investigated the effect of Ürkmez dam breach parameters on the generated maximum flood hydrograph by a two-dimensional version of HEC-RAS software. The results showed that the Froehlich relation has reasonable results for estimating the fracture parameters of the Ürkmez dam and the breach time parameter is one of the factors affecting the maximum discharge and the time to reach it.

Despite extensive research conducted on dam break, it is still important to predict characteristics of the flow caused by sudden dam break, including the water free surface profile and wave propagation velocity. The reservoir geometric shapes and the presence of downstream obstacles are among the effective parameters in the formation of the flow pattern. Thus, in this research, a comprehensive study of these parameters and hydrodynamics of the flow caused by dam break, with more details on the flow around downstream obstacles using different reservoir geometric shapes and three-dimensional numerical modelling, has been carried out.

2. Materials and Methods

2.1 Mathematical Model and Governing Equations

A three-dimensional incompressible and viscous fluid flow is governed by the continuity (conservation of mass) equation expressed as Eq. (1) and a set of momentum equations called the Navier-Stokes equations expressed as Eq. (2) to (4). Since the flow regime is turbulent, the turbulence terms have been appended to the Navier-Stokes equations. The Reynolds-averaged Navier-Stokes (RANS) equations in the Cartesian coordinate system (x, y, z) are used to achieve this objective [23].

$$\frac{\partial \bar{U}}{\partial x}+\frac{\partial \bar{V}}{\partial y}+\frac{\partial \bar{W}}{\partial z}=0 \tag{1}$$

$$\begin{aligned}\rho\left(\frac{\partial \bar{U}}{\partial t}+\bar{U}\frac{\partial \bar{U}}{\partial x}+\bar{V}\frac{\partial \bar{U}}{\partial y}+\bar{W}\frac{\partial \bar{U}}{\partial z}\right)&\\ =\rho g_x-\frac{\partial \bar{P}}{\partial x}+\mu\nabla^2\bar{U}&\\ -\rho\left(\frac{\partial \overline{\acute{u}^2}}{\partial x}+\frac{\partial \overline{\acute{u}\acute{v}}}{\partial y}+\frac{\partial \overline{\acute{u}\acute{w}}}{\partial z}\right)&\end{aligned} \tag{2}$$

$$\begin{aligned}\rho\left(\frac{\partial \bar{V}}{\partial t}+\bar{U}\frac{\partial \bar{V}}{\partial x}+\bar{V}\frac{\partial \bar{V}}{\partial y}+\bar{W}\frac{\partial \bar{V}}{\partial z}\right)&\\ =\rho g_y-\frac{\partial \bar{P}}{\partial y}+\mu\nabla^2\bar{V}&\\ -\rho\left(\frac{\partial \overline{\acute{u}\acute{v}}}{\partial x}+\frac{\partial \overline{\acute{v}^2}}{\partial y}+\frac{\partial \overline{\acute{v}\acute{w}}}{\partial z}\right)&\end{aligned} \tag{3}$$

$$\begin{aligned}\underbrace{\rho\left(\frac{\partial \bar{W}}{\partial t}+\bar{U}\frac{\partial \bar{W}}{\partial x}+\bar{V}\frac{\partial \bar{W}}{\partial y}+\bar{W}\frac{\partial \bar{W}}{\partial z}\right)}_{1}&\\ =\underbrace{\rho g_z-\frac{\partial \bar{P}}{\partial z}}_{2}+\underbrace{\mu\nabla^2\bar{W}}_{3}&\\ \underbrace{-\rho\left(\frac{\partial \overline{\acute{u}\acute{w}}}{\partial x}+\frac{\partial \overline{\acute{v}\acute{w}}}{\partial y}+\frac{\partial \overline{\acute{w}^2}}{\partial z}\right)}_{4}&\end{aligned} \tag{4}$$

In the equations above, $\bar{U}$, $\bar{V}$, and $\bar{W}$ are average velocities, respectively along x, y, and z axes, and g_x, g_y, and g_z represent gravitational accelerations along the coordinate axes. Each term in the Navier-Stokes equations represents a

specific physical behavior of the fluid flow. As indicated in Eq. (4), terms 1 to 4 are called Convection, Source, Diffusion, and the Reynolds stress terms, respectively. The governing equations are solved using the finite volume method in FLOW-3D software [24].

2.2 Model Geometry

In this research, six reservoirs with different geometries, including wide, trapezoidal, L-shaped, long, hexagonal, and octagonal reservoirs, have been used to investigate the effect of the reservoir geometric shape on the flow caused by dam break around an obstacle located downstream. In order to achieve identical situations, the volumes of all reservoirs and the lengths of the downstream channels connected to them are assumed equal. A cylindrical pier with a diameter of 0.04 m and a central distance of 1.08 m from the gate has been established in the downstream channels connected to reservoirs shown in Fig.1. The schematic plans of the reservoirs and downstream channels in the presence of the obstacle are shown in Figs. 1 and 2. The downstream bed is dry for all models, and the initial level of water in the reservoir is assumed to be 0.4 m. The origin of the coordinates system is located at the center of the gate so that it is along the positive direction of the x-axis along with the flow. The coordinates of the gauge points selected to investigate the water level, velocity profile, and pressure variation have been stated in Table 1.

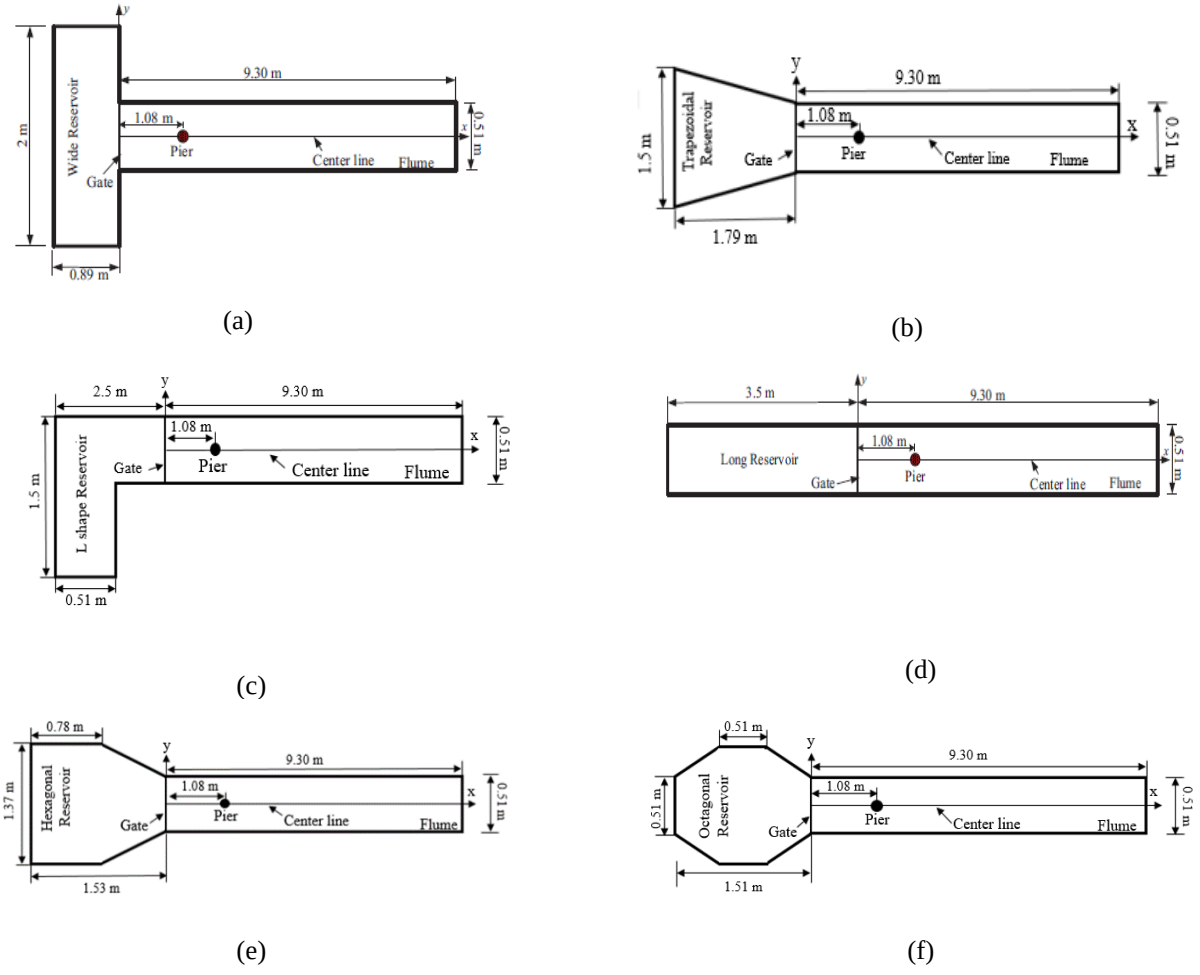

Fig. 1: Schematic plans of the reservoirs and the channels connected to them – (a) Wide res., (b) Trapezoidal res., (c) L-shaped res., (d) Long res., (e) Hexagonal res., and (f) Octagonal res.

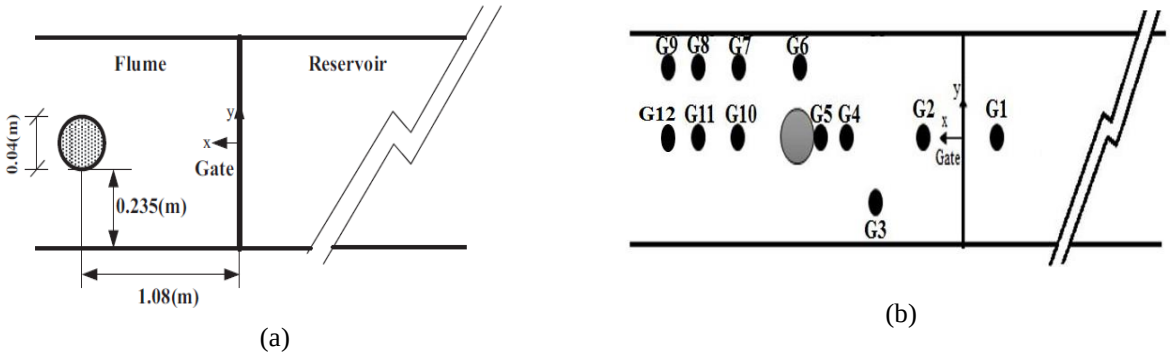

Fig. 2: Schematic plan of the downstream channel – (a) Pier location and (b) Selected gauge points

Table. 1: Cartesian coordinates of gauge points

Gauge point	x (m)	y (m)
G1	-0.15	0
G2	0.15	0
G3	0.83	-0.1175
G4	0.98	0
G5	1.06	0
G6	1.08	0.1175
G7	1.33	0.1175
G8	1.48	0.1175
G9	1.58	0.1175
G10	1.33	0
G11	1.48	0
G12	1.58	0

2.2 Model Geometry

The initial and boundary conditions used in numerical modeling are as follows:

-At the initial moment, for all models, all velocities are assumed zero.

-The walls and bottom of the reservoirs are assumed as wall (no-slip) boundary conditions.

-The fluid inside the reservoirs is defined as water and air.

-For the outlet flow, the outflow boundary condition is used.

-For variations along with the channel depth and width, the symmetry boundary condition is used individually for each direction.

Before presenting the results, the model's sensitivity to the mesh size and turbulence model was analyzed, and the numerical results were compared with the experimental data presented by Feizi et al. [7]. In this study, four mesh sensitivity analyses were performed. Fig. 3 shows the water-depth evolution with time where the measurements are compared to the numerical simulations for mesh sizes of 0.01, 0.03, 0.05, and 0.1 m. Based on the obtained values, the calculated RMSE (Root-Mean-Squared-Error) is presented in Table 2. The mesh size of 0.01 m shows the best fit compared to the others with the experimental values. Using three well-known turbulence models $k-\varepsilon-\text{standard}$, $k-\omega$, and $k-\varepsilon-RNG$, the water level changes were compared with laboratory values at G1 and G5 points.

By comparing the results obtained from different turbulence models, the RNG (Reynolds Normalized Groups) model was used, which is a highly recommended turbulence model for dam break simulation by numerous references [6, 7, 16, 17].

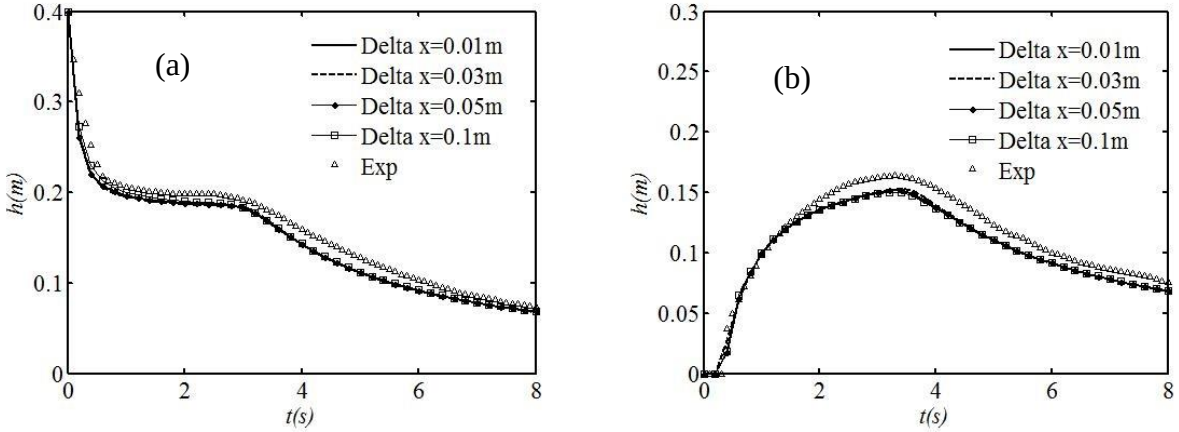

Fig. 3: Sensitivity analyses for different mesh sizes at (a) point G1 and (b) point G5 (Long reservoir test without pier) based on water level

Table. 2: Calculated RMSE for different mesh sizes in 3D numerical simulation

	Delta x=0.02	Delta x=0.03	Delta x=0.05	Delta x=0.1
G1	0.014	0.014	0.014	0.012
G5	0.008	0.010	0.010	0.011

3. Results and Discussion

3.1 Water Surface Profile Analysis

In order to obtain the water surface profile in a rectangular channel assuming the reservoir is full and infinite, Ritter's analytical solution is used. Therefore, the water level variation is obtained using the following equation:

$$Z = \left[\frac{1}{3}\left(2 - \frac{X}{T}\right)\right]^2, \quad (5)$$

where X and Z are dimensionless spatial coordinates corresponding to the longitudinal position and depth, respectively. These quantities are defined as $X = x/h_0$ and $Z = h/h_0$, where x is the distance from the gate, h_0 is the initial water level in the reservoir, and h is the water level which is calculated numerically. The time dimensionless quantity is also defined as $T = t\sqrt{g/h_0}$, where t is the elapsed time and g is the gravitational acceleration.

To attain a better comparison, the results related to water surface profiles at points G1, G2, G4, G6, G10, G11 are represented as dimensionless plots in Fig. 4. In these plots, the horizontal and vertical axes indicate the dimensionless time and flow depth, respectively. Comparing the three-dimensional numerical model results with Ritter's analytical solution is restricted to the time interval $T = 0$ to $T = 15$. After this time period, the water level in the reservoirs encounters a decreasing trend caused by drainage, since the reservoirs are always assumed full in Ritter's analytical solution. For the long reservoir and in the absence of the obstacle, a one-dimensional flow is formed downstream. Thus, the long reservoir is considered as the basis of comparison between the results of the other reservoirs. The water level variation in the reservoirs compared with the long reservoir is shown in Fig. 4. Besides, the water level difference percentage for each reservoir compared to the long reservoir is given in Table 3.

According to Fig. 4 and the flood wave motion illustrated in Fig. 5, from the beginning of the reservoir wall to near the obstacle (points G1-G3), the water level variation is mainly affected by reservoir geometric shapes, and the presence of the obstacle does not have a significant effect on the water level. Thus, the formation of cross-waves in the downstream channels connected to the wide, trapezoidal, hexagonal, and octagonal reservoirs causes the formation of a two-dimensional flow pattern. Due to the abrupt contraction in the wide reservoir, the transversal velocity components emerging in the downstream channel connected to the wide reservoir are greater than those corresponding to the other reservoirs. The octagonal and hexagonal reservoirs have a trend similar to the wide reservoir. The difference is that most water level fluctuations after the wide reservoir are observed in the octagonal reservoir followed by the hexagonal one. This is due to the longer conversion length in the hexagonal reservoir than the octagonal one, so water level fluctuations due to the cross-section change in the hexagonal reservoir are less than the octagonal one. Due to the geometric shape of the L-shaped and long reservoirs, the dominant flow pattern in these reservoirs is one-dimensional and less fluctuations are observed on the water surface. As the flow collides with the obstacle, in addition to the effect of the reservoir geometric shape, the effect of the obstacle also appears. According to the results, the flow created in the wide reservoir downstream channel has the largest difference percentage with a value of 13.91%, followed by the octagonal, hexagonal, and trapezoidal reservoirs with values of 12.72%, 10.76%, and 9.78%, respectively.

Eventually, for the L-shaped reservoir, the difference percentage is as low as 1.41%, which originates from the fact that flows created in the long and L-shaped reservoirs are very similar.

The results showed that the Ritter analytical solution is closer to the values obtained from the Long reservoir. Similar to the assumptions made in Ritter's analytical solution, this is because there is a one-dimensional flow in this reservoir. The differences between the conditions in which the pier is present and absent in the downstream channels connected to different reservoirs at different points are given in Table 4. As it is obvious, a portion of fluctuations at different points is caused by reservoir geometric shapes, and the other portion is related to the presence of the pier.

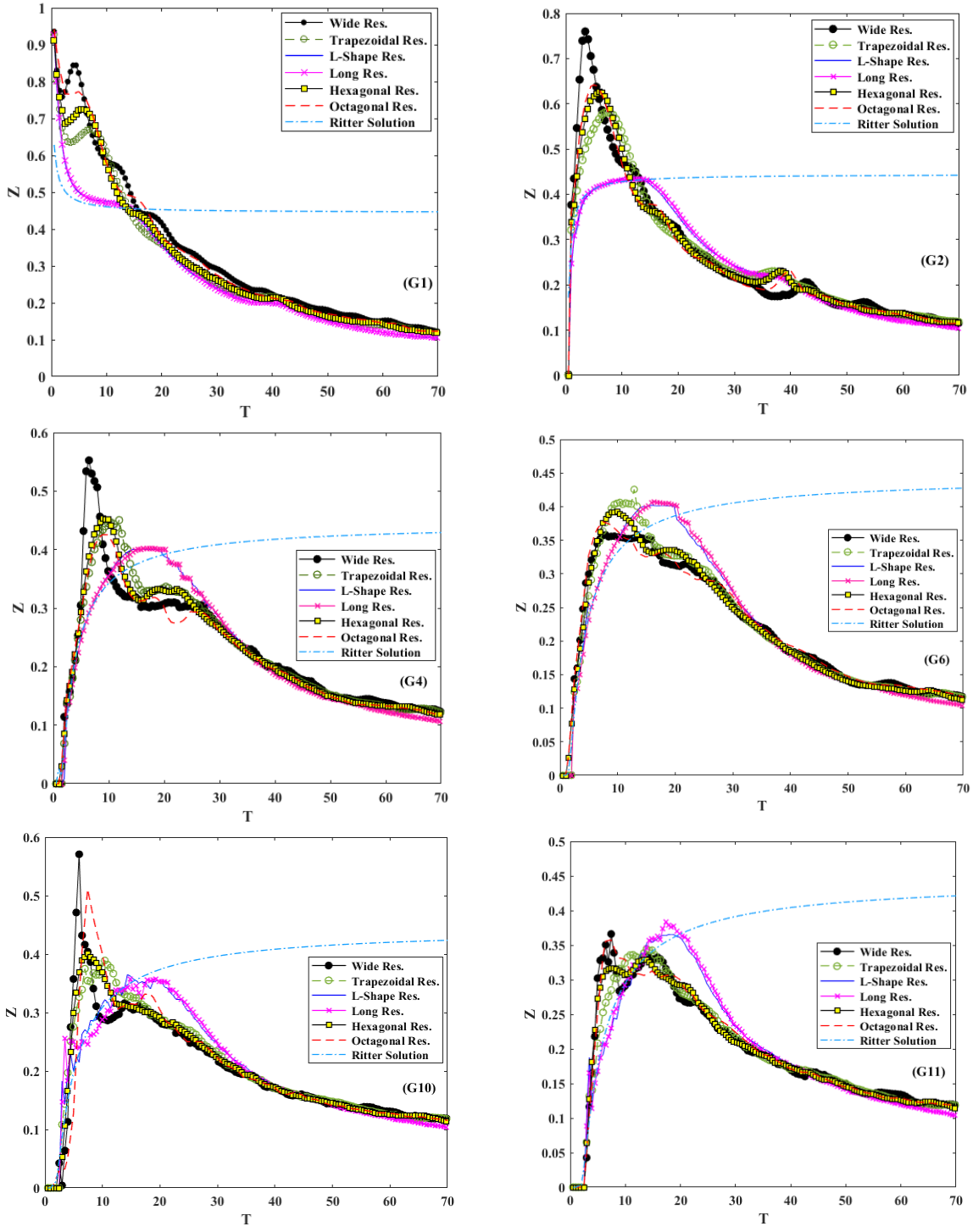

Fig. 4: Water surface profile variation for different reservoirs at different points

Table. 3: Water level difference percentage for each reservoir and Ritter's analytical solution compared to the long reservoir in the presence of the obstacle downstream

Gauge point	Wide res.	Trapezoidal res.	L-shaped res.	Hexagonal res.	Octagonal res.	Ritter's solution
G1	21.09	11.41	0.96	12.37	17.02	1.76
G2	15.04	11.44	0.98	12.54	13.81	0.90
G4	12.80	9.40	1.10	10.06	10.39	1.06
G6	9.70	7.94	1.26	8.47	11.33	1.22
G10	12.89	9.53	2.50	10.78	12.90	2.07
G11	11.93	8.93	1.64	10.33	10.85	1.30

Table. 4: Water level difference percentages for reservoirs in the presence and absence of the obstacle downstream

Gauge point	Wide res.	Trapezoidal res.	L-shaped res.	Long res.	Hexagonal res.	Octagonal res.
G1	2.90	3.59	4.73	4.82	3.19	4.48
G3	9.40	6.80	9.38	9.05	7.86	7.99
G4	13.87	10.24	12.53	11.67	10.73	9.02
G6	11.13	7.39	10.14	9.82	9.07	9.77
G10	9.18	6.02	8.49	5.97	8.02	10.35
G11	7.97	3.97	4.72	4.44	4.54	4.58

According to Fig. 5, it is concluded that the effect of the pier on the flow caused by dam break is local and only significant over a certain length behind the pier. At this certain length, wake vortices initially form at a longer distance behind the pier, but they move toward the pier, causing the length to decrease over time. In other words, at a certain approximate length behind the obstacle, a combined flow composed of the outflow of different-shaped reservoirs and the reflective flow due to the presence of the obstacle is formed. The approximate value of the effective length, in which the flow is affected, depends on the reservoir geometric shape. Thus, the maximum length is related to the wide reservoir and the lowest length is related to the long reservoir. The effective length is approximately 22.5 and 21.5 times the pier diameter for the wide and octagonal reservoirs, respectively. For the hexagonal and trapezoidal reservoirs, the effective length is approximately identical and 20.5 times the pier diameter. Eventually, for the L-shaped and long reservoirs, this length obtained is the same and 19.5 times the pier diameter.

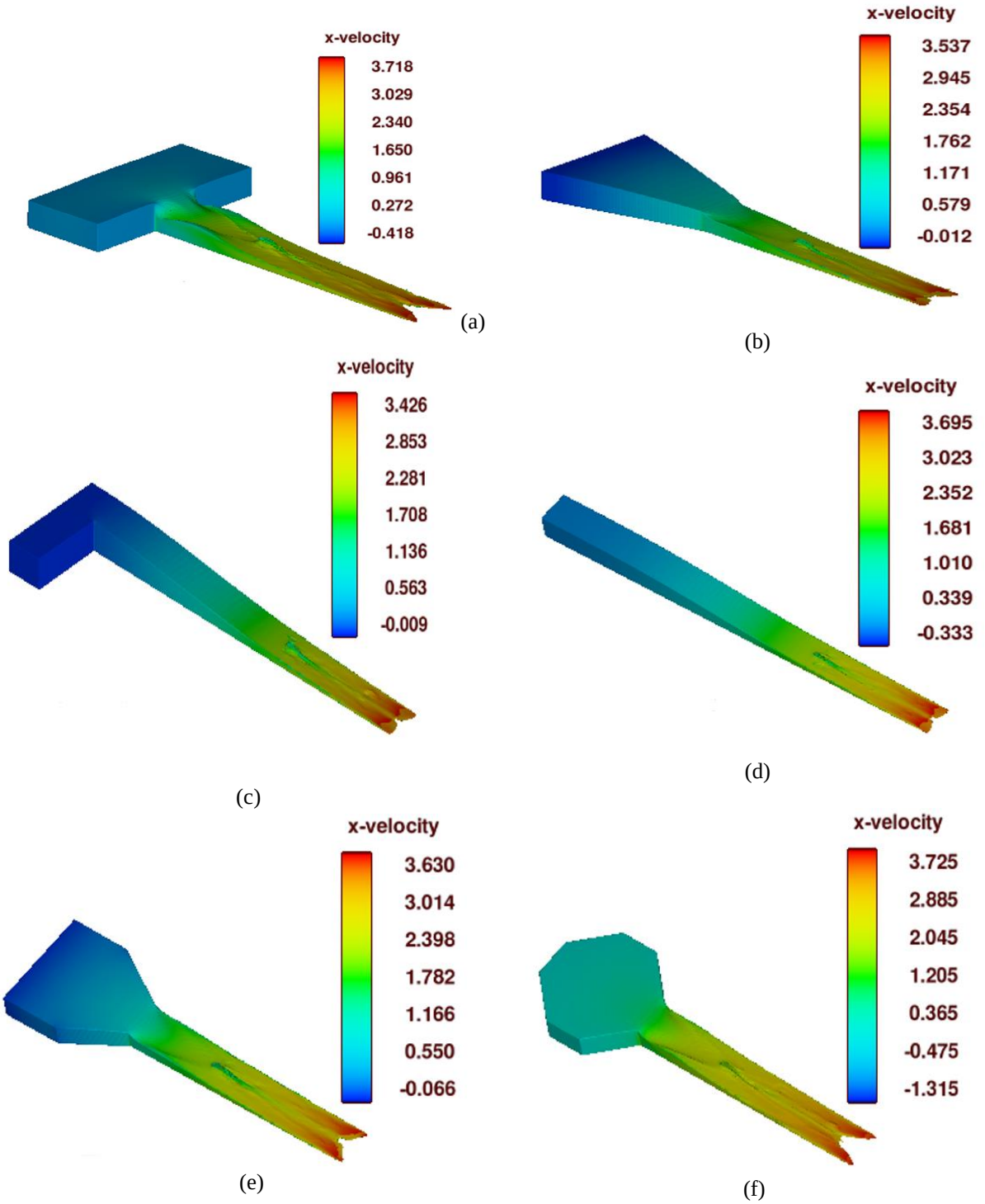

Fig. 5: Flood wave motion in the downstream channel around the obstacle at $t = 1$ s – (a) Wide res., (b) Trapezoidal res., (c) L-shaped res., (d) Long res., (e) Hexagonal res., and (f) Octagonal res.

Figure 6 shows the peak water level and wave fluctuations caused by the flow at the points located on the channel centerline (G2, G4, G5, G10, and G11) and also out of the channel centerline (G3, G6, G7, G8, and G9). The dimensionless peak water level (h_p/h_0) is plotted versus the dimensionless distance of the points from the gate ($x/c_0 t_p$), where $c_0 = \sqrt{gh_0}$ and t_p is the corresponding time to the peak water level. According to the plots, at the points located out of the centerline, water level fluctuations for all reservoirs are weak because due to the collision of the flow with the obstacle, the concentration and intensity of wake waves are mostly at the channel central axis and a low number of fluctuations reaches the other points. Also, by moving away from the gate, the cross waves created in the wide, octagonal, hexagonal, and trapezoidal reservoirs become weaker. As a result, the fluctuations caused by the reservoir geometric shape are small. At the points located on the centerline, due to the high concentration and intensity of

wake waves, fluctuations are significant for all reservoirs. The fluctuations caused by the collision of the flow with the pier combine with the fluctuations created due to the reservoir shape. The combination of these fluctuations is larger for the wide reservoir compared to the other ones due to the two-dimensional flow pattern. For the octagonal, hexagonal, and trapezoidal reservoirs, the situation is similar to the wide reservoir but with a lower intensity. For the long and L-shaped reservoirs, due to the one-dimensional flow pattern, the fluctuations caused by the reservoir shape are insignificant and limited to wake waves behind the obstacle caused by the collision of the flow with the pier

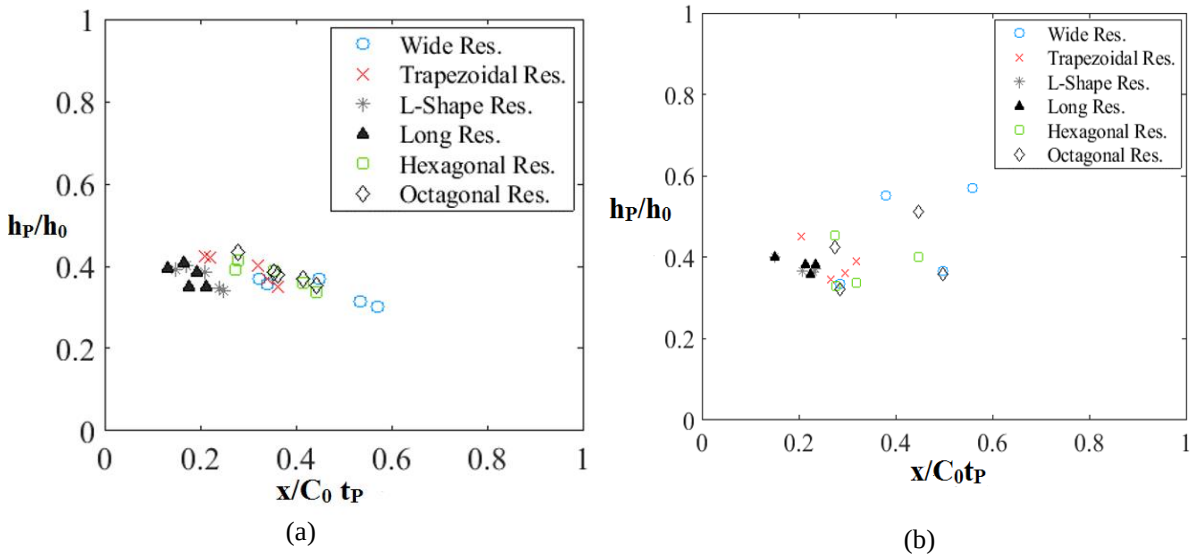

Fig. 6: Peak water level at points located (a) out of the centerline and (b) on the centerline

3.2 Velocity Profile Variations Analysis

Figure 7 shows the velocity distribution over the depth obtained from the three-dimensional numerical model and Ritter's analytical solution at points G3 and G10, which are located before and after the pier at times $t = 2$ s and $t = 4$ s. Table 5 also indicates the velocity difference percentage of each reservoir compared to the long reservoir at points G3 and G10. In Fig. 7, the horizontal and vertical axes indicate the dimensionless velocity $(U = \frac{2}{3}(1 + \frac{X}{T}))$ and dimensionless depth $(Z = h/h_0)$, respectively. As it is observed, in the three-dimensional model, the velocity starts from zero on the bed and approaches a certain value away from the wall. While in Ritter's analytical solution, the velocity distribution is assumed uniform along with the depth. Due to the effect of the reservoir geometric shape on the flow pattern, velocity fluctuations are obviously seen in Fig.7. For the wide, octagonal, hexagonal, and trapezoidal reservoirs, which experience a two-dimensional flow due to the formation of cross-waves, higher velocity fluctuations are obtained. At point G10, which is located behind the pier, the formation of back flow originates from collision of the flow with the pier, the effects of wake vortices and high turbulence, and the fluctuations related to the reservoir shape can be observed.

Table. 5: Velocity difference percentages in channels connected to each reservoir compared to the long reservoir in the presence of the obstacle downstream

Gauge point	Time (seconds)	Wide res.	Trapezoidal res.	L-shaped res.	Hexagonal res.	Octagonal res.
G3	2	3.11	6.21	0.37	1.12	0.62
G3	4	6.67	18.33	1.67	11.67	10.0
G10	2	5.74	4.92	1.64	3.11	9.34
G10	4	5.43	2.17	1.09	6.52	8.70

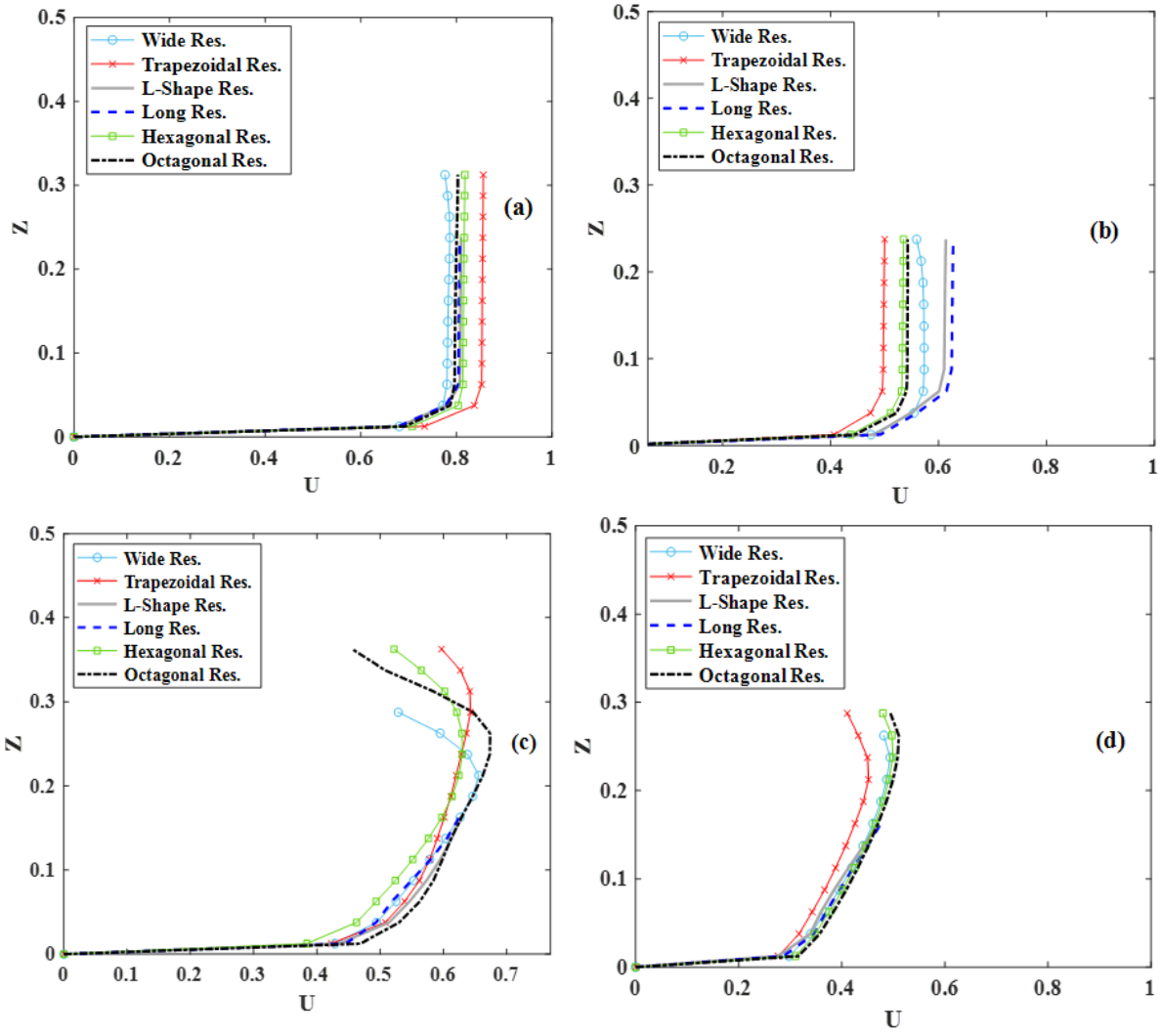

Fig. 7: Velocity distribution over the depth at point G3 (a) $t = 2$ s, (b) $t = 4$ s, and point G10 (c) $t = 2$ s, and (d) $t = 4$ s

3.3 Pressure Variations Analysis

Figure 8 shows the pressure variation along with the depth for different reservoir shapes at point G5 (on the pier) at different moments. According to this figure, at point G5, at the first second, the maximum pressure is related to the wide reservoir followed by the octagonal and hexagonal reservoirs, respectively. The minimum pressure is related to the L-shaped and long reservoirs. The trapezoidal reservoir stands in the middle of these two states. Actually, for the wide, octagonal, and hexagonal reservoirs, the pressure reaches its peak value just when the flow enters downstream suddenly, at an approximate water level of 0.12 m. At the initial flow entry moment, due to the effect of these reservoir geometries, cross waves with a higher peak velocity compared to other reservoir geometries enter the downstream channel, which leads to an increase in pressure for these reservoirs. The effect of the reservoir geometric shape on the flow pattern attenuates gradually over time as it reaches the third second, so the velocity and consequently the pressure decreases. For the L-shaped and long reservoirs, due to the constant cross-section and approximately one-dimensional flow, the velocity and consequently the pressure increases gradually. Over time, the flow energy decreases, and as fluctuations are damped, the flow velocity reaches its previous value. The velocity variation becomes negligible, so at the tenth second from the flow entry moment to the downstream channel, the pressure attains a constant value over the reservoir. At this point, the pressure variation is curved because this point is affected by the pier and the reflective flow from it.

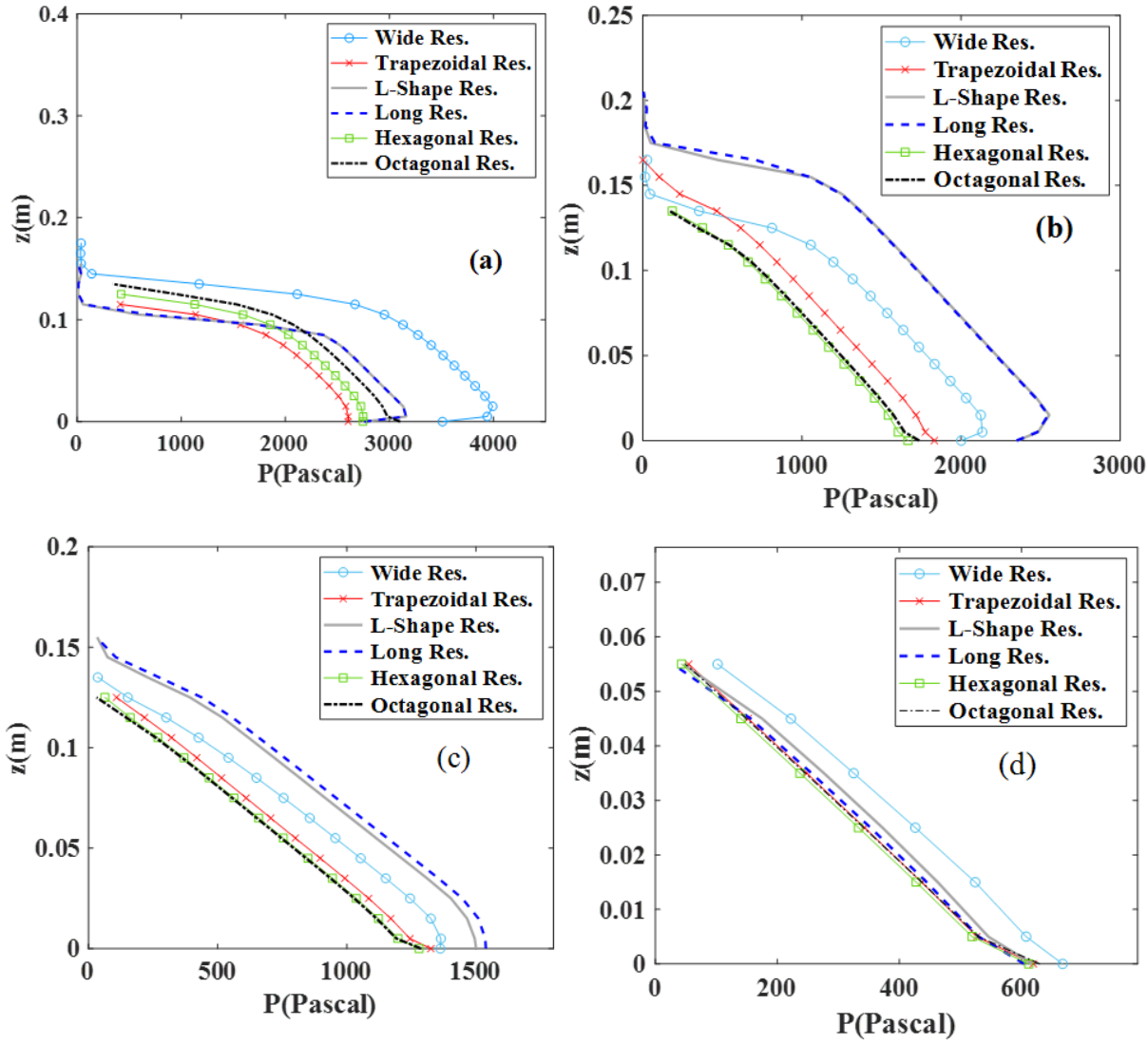

Fig. 8: Pressure variation along the depth at point G5 at (a) $t = 1$ s, (b) $t = 3$ s, (c) $t = 5$ s, and (d) $t = 10$ s

4. Conclusion

In this research, hydrodynamic characteristics of the flow caused by dam break around a downstream obstacle considering different reservoir geometric shapes and a downstream dry bed were investigated. Thus, six reservoirs with different geometries, including wide, trapezoidal, L-shaped, long, hexagonal, and octagonal reservoirs, were connected to the downstream channel individually. The simulations were performed in FLOW-3D software. Some of the important characteristics of the flow, including the water level profile, vertical velocity distribution profile, pressure variation along with the depth, and flood wave motion were obtained from the numerical modeling and compared with each other. Among the modeled reservoirs, the wide, octagonal, hexagonal, and trapezoidal reservoirs, due to their geometric shapes, cause the cross waves formation downstream and transform the flow pattern to a two-dimensional flow. For long and L-shaped reservoirs, due to the alignment of the reservoir with the downstream channel, approximate one-dimensional flow patterns are created after the collision with the downstream obstacle, the outflow of the reservoirs is affected by both reservoir geometric shapes and the presence of the obstacle. The results showed that the effect of the reservoir geometric shape on the flow caused by dam break could be observed along the entire length of the channel. In contrast, the effect of the obstacle is local and can be seen along a certain length in the area behind the obstacle. Among the mentioned reservoirs, the strongest fluctuations are created by the wide reservoir, and the weakest fluctuations are related to the long and L-shaped ones. Furthermore, the maximum and minimum length behind the obstacle, in which the flow is affected by the presence of the pier, is obtained in the channels connected to the wide and long reservoirs, respectively.

References

[1] Issakhov A, Zhandaulet Y, Nogaeva A (2018) Numerical simulation of dam break flow for various forms of the obstacle by VOF method. Int. J. Multiph. Flow 109. https://doi.org/10.1016/j.ijmultiphaseflow.2018.08.003

[2] Issakhov A, Imanberdiyeva M (2019) Numerical simulation of the movement of water surface of dam break flow by VOF methods for various obstacles. Int. J. Heat Mass Transf. 136:1030-1051. https://doi.org/10.1016/j.ijheatmasstransfer.2019.03.034

[3] Soares-Frazão S, Zech Y (2002) Dam break in channels with 90° bend. J. Hydraul. Eng. 128(11):956-968. https://doi.org/10.1061/(ASCE)0733-9429(2002)128:11(956)

[4] Soares-Frazão S (2007) Experiments of dam-break wave over a triangular bottom sill. J. Hydraul. Res. 45:19-26. https://doi.org/10.1080/00221686.2007.9521829

[5] Soares-Frazão S, Zech Y (2007) Experimental study of dam-break flow against an isolated obstacle. J. Hydraul. Res. 45:27-36. https://doi.org/10.1080/00221686.2007.9521830

[6] Ozmen-Cagatay H, Kocaman S (2011) Dam-Break flow in the presence of obstacle: Experiment and CFD simulation. Eng. Appl. Comput. Fluid Mech. 5(4):541-552. https://doi.org/10.1080/19942060.2011.11015393

[7] Feizi Khankandi A, Tahershamsi A, Soares-Frazão S (2012) Experimental investigation of reservoir geometry effect on dam-break flow. J. Hydraul. Res. 50(4):376-387. https://doi.org/10.1080/00221686.2012.690974

[8] Aureli F, Dazzi S, Maranzoni A, Mignosa P, Vacondio R (2015) Experimental and numerical evaluation of the force due to the impact of a dam-break wave on a structure. Adv. Water Resour. 76:29-42. https://doi.org/10.1016/j.advwatres.2014.11.009

[9] Costabile P, Macchione F, Natale L, Petaccia G (2015) Comparison of scenarios with and without bridges and analysis of backwater effect in 1-D and 2-D river flood modeling. Comput. Model. Eng. Sci. 109-110(2):81-103. https://doi.org/10.3970/cmes.2015.109.081

[10] Hooshyaripor F, Tahershamsi A (2015) Effect of reservoir side slopes on dam-break flood waves. J. Eng. Appl. Comput. Fluid Mech. 9(1):458-468. https://doi.org/10.1080/19942060.2015.1039630

[11] Javadian M, Kaveh R, Mahmoodinasab F (2016) A Study on Experimental Model of Dam Break Problem and Comparison Experimental Results with Analytical Solution of Saint-Venant Equations. Int. J. Adv. Biotechnol. Res. 7:1239-1245.

[12] Jian W, Liang D, Shao S, Chen R, Yang K (2016) Smoothed particle hydrodynamics simulations of Dam-Break flows around movable structures. Int. J. Offshore Polar Eng. 26(1). https://doi.org/10.17736/ijope.2016.ak08

[13] Moradi Mofrad B, Barnjani S, Safari A (2017) Modeling of Turbulent Flow Due to the Dam Break against Trapezoidal Barrier. J. Civ. Eng. Mater. Appl. 1(1). https://doi.org/10.15412/J.JCEMA.12010104

[14] Yilmaz A, Dal K, Demirci M, Kocaman S (2017) Numerical Investigation of Dam-Break Flow over a Bottom Obstacle Using Eulerian Finite Element Method. Int. J. Adv. Eng. Res. Sci 4(12):203-208. https://doi.org/10.22161/ijaers.4.12.30

[15] Amini A, Arya A, Eghbalzadeh A, Javan M (2017) Peak flood estimation under overtopping and piping conditions at Vahdat Dam, Kurdistan Iran. Arabian Journal of Geosciences, 10(6). http:// doi.org/10.1007/s12517-017-2854-y

[16] Azimi H, Heydari M, Shabanlou S (2018) Numerical simulation of the effects of downstream obstacles on malpasset dam break pattern. J. Appl. Res. Water Wastewater 10:441-446. https://doi.org/10.22126/arww.2018.1007

[17] Feizi A (2018) Hydrodynamic Study of the Flows Caused by Dam Break around Downstream Obstacles. Open Civ. Eng. J. 12:225-238. https://doi.org/10.2174/1874149501812010225

[18] Saghi H, Lakzian E (2019) Effects of using obstacles on the dam-break flow based on entropy generation analysis. Eur. Phys. J. Plus 134(5):134-237. https://doi.org/10.1140/epjp/i2019-12592-3

[19] Wang B, Zhang J, Chen Y, Peng Y, Liu X, Liu W (2019) Comparison of measured dam-break flood waves in triangular and rectangular channels. J. Hydrol. 575:690-703. https://doi.org/10.1016/j.jhydrol.2019.05.081

[20] Monteiro LR., Lucchese LV, Schettini C EB (2019) Comparison between hydrostatic and total pressure simulations of dam-break flows. Journal of Hydraulic Research, 58(5): 725–737. https://doi.org/10.1080/00221686.2019.1671509.

[21] Kocaman S, Güzel H, Evangelista S, Ozmen-Cagatay H, Viccione G (2020) Experimental and Numerical Analysis of a Dam-Break Flow through Different Contraction Geometries of the Channel. J. Water 12(4). https://doi.org/10.3390/w12041124

[22] Najar M, GÜL A (2022) Investigating the Influence of Dam-Breach Parameters on Dam-Break Connected Flood Hydrograph. Teknik Dergi. 796334. https://doi.org/ 10.18400/tekderg.

[23] Toro, E.F. (2000). Shock Capturing Methods for Free Flows. John Wiley and Sons.

[24] FLOW-3D User's Manual (2011) Version 10.0. Flow Science, Inc.